

## Long slender drops in a simple shear flow

By E. J. HINCH

Department of Applied Mathematics and Theoretical Physics,  
Cambridge University, England

AND A. ACRIVOS

Chemical Engineering, Stanford University, U.S.A.

(Received 27 March 1979)

We study theoretically the slow viscous motion of a long slender drop placed in a simple shear flow, the drop having a low viscosity compared with that of the suspending fluid. As a simplifying approximation, the cross-section of the drop is taken to be circular. An equilibrium shape with the drop nearly aligned with the flow is found for all shear rates, although the equilibrium is only stable to small disturbances for shear rates below some critical value. The stable equilibria just below the critical shear rate are found to be accessible only if the shear rate is increased slowly.

---

### 1. Introduction

The deformation and break-up of a single drop of viscosity  $\mu_i$  freely suspended in another fluid of viscosity  $\mu$  undergoing shear at vanishingly small Reynolds number has been the subject of several studies theoretical as well as experimental. These studies have established that drops of low viscosity relative to the suspending fluid, i.e.  $\mu_i \ll \mu$ , can deform into long and slender shapes, in contrast to the case  $\mu_i \gtrsim \mu$  where the drop remains more or less spherical up to the point of break-up. Such slender drops require relatively large shear rates before they break, and for this reason have attracted the attention of several investigators.

Two recent theoretical studies (Acricos & Lo 1978; Hinch & Acricos 1979) have presented solutions for the two undisturbed flows, axisymmetric extensional flow and two-dimensional hyperbolic flow respectively, both of which are pure straining motions. In this paper we extend these analyses to simple shear flow, not only for completeness, but also because most experiments have been performed for this flow which is easier to set up. At first glance, it might appear that the present analysis could follow the general lines of the earlier studies and that the results for simple shear would not differ much from those for the pure straining flows. We shall see, however, that the presence of the vorticity in the undisturbed flow gives rise to some fundamental differences.

We recall that in our analysis of hyperbolic flow (Hinch & Acricos 1979), we decomposed the undisturbed two-dimensional strain into an axisymmetric strain plus a remainder which was then treated as a perturbation. The regular perturbation expansion appeared to converge rapidly, and, although the cross-section of the drop was found to be approximately an ellipse with an axis ratio of 1.5, the deformation curve of the drop length versus shear rate, as well as the critical strain rate required for the

break-up, were essentially identical to those obtained by Acrivos & Lo (1978) for the axisymmetric flow with a drop of circular cross-section. In retrospect, the result is hardly surprising. The length of the drop is determined in the two flows by the same dynamical balance between surface tension and the stretching due to the component of the strain rate along the slender drop. The difference between the axisymmetric convergence of the undisturbed flow in the cross-section and the non-axisymmetric convergence in the hyperbolic flow is easily accommodated by a small change in the cross-sectional shape which has an indirect effect on the dynamics that determine the length only through the resulting very small change in the cross-sectional area.

In view of the above, one might be tempted to develop a solution to the present problem by first decomposing the undisturbed simple shear into a two-dimensional straining motion, with its principal axes of strain at  $45^\circ$  to the direction of the flow, plus a solid-body rotation, and then treat the latter as a perturbation. Experiments have shown, however (see e.g. Torza, Cox & Mason 1972), that the long axis of slender drops is almost aligned with the flow rather than being slightly perturbed from the principal axis of strain. Thus the vorticity plays a role more significant than that of a perturbation, and so the scheme suggested above is bound to fail, unless perhaps a large number of terms in the expansion could be obtained.

We have chosen, therefore, an alternative approach in which we do not alter the form of the shear flow, but make the approximation that the drop has a circular local cross-section. In § 2, we shall derive equations governing the location of the curved centre-line of the drop as well as the variation of the local radius, but shall ignore all the velocity and stress fields which would deform the cross-section from its assumed circular form. Unfortunately, the present analysis for simple shear flow, in contrast to the hyperbolic flow we studied earlier, cannot be incorporated into a rational perturbation scheme, and thus we are unable to estimate by how much the local cross-section departs from being circular. But, based on our earlier results in hyperbolic flow that the cross-section does not change greatly from being circular, and that the deformation curve and critical shear rate differ very little from those calculated with a circular cross-section for axisymmetric flow, we have some confidence that our assumption of a circular cross-section in simple shear will not lead to any significant errors. Besides, our *ad hoc* assumption that the cross-section is circular greatly simplifies the problem in that it enables us to analyse easily several aspects of the dynamics of the drop and to make predictions which are in reasonable agreement with experiments. On the other hand, any theory which did not assume that the cross-section is circular would be considerably more difficult to develop and would inevitably require a large computation effort probably beyond the capabilities of present-day computers.

In this paper we shall show that the behaviour of a low-viscosity drop in simple shear differs substantially from that found earlier in pure straining flows. First the inclination of the axis of the drop to the direction of flow, which has been observed in experiments to decrease as the drop lengthens in stronger flows, will be shown to be of the same order of magnitude as the slenderness of the drop. This small inclination greatly reduces the effective strength of the straining motion stretching the drop and results in the non-dimensional length taking a form  $l(\mu_i/\mu)^{\frac{1}{2}}/a$  and being a function of a non-dimensional shear rate  $G = E\mu a(\mu_i/\mu)^{\frac{2}{3}}/\gamma$ , in which  $E$  is the shear rate,  $l$  the half-length of the drop,  $a$  the radius of a spherical drop with the same volume, and  $\gamma$  the interfacial tension. These non-dimensional forms which are derived in § 2 were

given earlier by Acrivos & Lo (1978). In contrast to the results for the pure straining flows, we shall find in § 3 that a steady shape drop exists for all shear rates. We shall then find in § 4.4 that the equilibrium is unstable to small disturbances if  $G > 0.0541$ . Thus, in shear flow, the critical flow strength is due to an instability to small disturbances, rather than a non-existence of steady drop shapes as in the pure straining flows. We will further find in § 4.5 that if the shear rate is suddenly increased beyond a certain value, then the drop will not reach the equilibrium shape corresponding to the new shear rate, even if this shape is stable to small disturbances. This instability to large disturbances may help to explain the large scatter in the experimentally measured values of critical shear rates, and the difficulty that has been experienced in obtaining reproducible data in simple shear when the drops are long and slender (Grace 1971). The different behaviour of a drop in simple shear and in pure straining flows will be seen to be due to the presence of vorticity which causes the slender drop to align itself in a direction of no straining and which leads to oscillations around an equilibrium. These differences in behaviour do not depend on how the flow converges in the cross-sectional plane, which in turn determines the cross-sectional shape. We therefore believe that the assumption of a circular cross-section can affect the theoretical predictions only in a minor way.

## 2. Governing equations

### 2.1. The co-ordinate system

We study the slow viscous motion of a drop with the undisturbed flow far from the drop taking the form of a simple shearing motion,

$$\mathbf{u} = (Ey, 0, 0),$$

with respect to the fixed Cartesian system  $(x, y, z)$ . We adopt the *ad hoc* approximation discussed in the introduction that the drop has a circular cross-section of radius  $R(x, t)$  and denote the displacement of its centre-line above the direction of the flow by  $\eta(x, t)$ , see figure 1. Because of symmetry about the origin,  $R(-x, t) = R(x, t)$  and  $\eta(-x, t) = -\eta(x, t)$ . Also  $l(t)$ , which is the first positive root of  $R(l, t) = 0$ , is the half-length of the drop. The equation for the surface of the drop is thus

$$z^2 + (y - \eta)^2 = R^2 \quad \text{for} \quad |x| \leq l(t).$$

We assume that the drop is slender and nearly aligned with the flow, so that

$$R, \eta \ll l \quad \text{and} \quad \partial R / \partial x, \partial \eta / \partial x \ll 1.$$

It is convenient to introduce local polar co-ordinates  $r, \theta$  with respect to the centre-line of the drop, so that

$$y = \eta + r \sin \theta, \quad z = r \cos \theta.$$

The co-ordinate system  $(x, r, \theta)$  is not orthogonal, however, because the unit vector for  $x$  increasing at fixed  $r$  and  $\theta$  has a small component in the  $yz$  plane. This slight skewness cannot be neglected, because it produces the vital stretching which keeps the drop long and slender. To a large extent we shall avoid the difficulties of working in a skew co-ordinate system, and only employ the skew co-ordinates to express concisely the results of our calculations in the original Cartesian system. Similarly, we

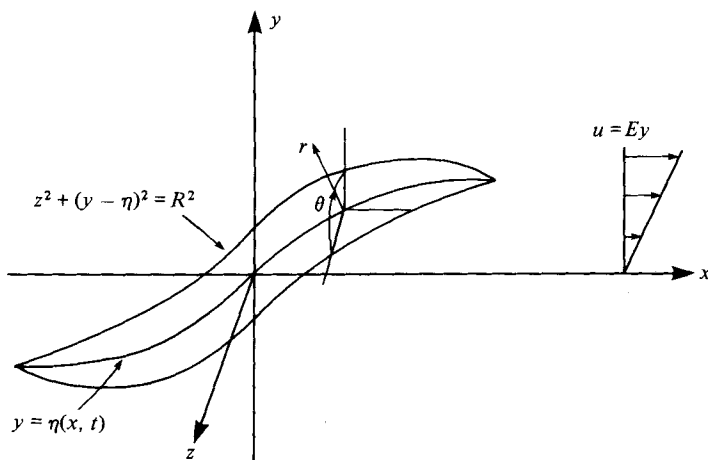


FIGURE 1. The co-ordinate system.

shall take components of vectors and tensors on the three unit vectors, expressed in terms of the Cartesian co-ordinate system

$$\hat{\mathbf{x}} = (1, 0, 0), \quad \hat{\mathbf{r}} = (0, \sin \theta, \cos \theta), \quad \hat{\boldsymbol{\theta}} = (0, \cos \theta, -\sin \theta),$$

where it should be noted that  $\hat{\mathbf{x}}$  is not the unit vector for the skew co-ordinate system.

In our polar co-ordinates the surface of the drop is

$$r = R(x, t) \quad \text{in} \quad |x| \leq l(t),$$

with a normal  $n_x = -R' - \eta' \sin \theta$ ,  $n_r = 1$ ,  $n_\theta = 0$ ,

where primes will be used to denote derivatives with respect to  $x$  and dots derivatives with respect to time. Although the normal shown above is not quite of unit length, this fact will cause no difficulties since  $\mathbf{n}$  will only be used in expressions which are homogeneous in it.

The undisturbed flow in our polar co-ordinates is then

$$u_x = E(\eta + r \sin \theta), \quad u_r = u_\theta = 0,$$

and its associated stress field is

$$\sigma_{xr} = \sigma_{rx} = \mu E \sin \theta, \quad \sigma_{x\theta} = \sigma_{\theta x} = \mu E \cos \theta,$$

all other components being zero.

## 2.2. The external flow

Since our analysis will be restricted to inertialess motions, the instantaneous shape of the drop determines the disturbance flow through the boundary condition on the stress, and the disturbance flow thus determined can then be used to find the evolution of the shape. To avoid the complications of the skew co-ordinates, we solve the Stokes equations of motion in the Cartesian system by expressing the disturbance flow outside the droplet in terms of singularities distributed along the centre-line of the drop.

As the fluid inside the drop has a low viscosity, it cannot exert any significant shear stress on the external fluid, and the disturbance flow must therefore cancel the

shear stress of the undisturbed flow on the surface of the drop. A suitable flow is generated by a line distribution of stresslets. Hence we consider distributed along the centre-line of the drop stresslets of strength  $4\pi\mu f(x)$ , which induce a flow

$$(u_x, u_y, u_z) = \int_{-l}^l \frac{\frac{3}{2}f(s)(x-s)(y-\eta(s))}{[(x-s)^2 + (y-\eta(s))^2 + z^2]^{\frac{3}{2}}} (x-s, y-\eta(s), z) ds,$$

and a pressure 
$$p = \int_{-l}^l \frac{3\mu f(s)(x-s)(y-\eta(s))}{[(x-s)^2 + (y-\eta(s))^2 + z^2]^{\frac{3}{2}}} ds,$$

where the time dependence of  $\eta$  has been suppressed. Evaluating the integrals asymptotically for the slender drop, we find that the flow near the drop,  $r = O(R)$ , is to leading order parallel to the undisturbed flow,

$$u_x \sim f(x) \frac{y-\eta(x)}{(y-\eta(x))^2 + z^2}, \quad u_y, u_z \sim 0,$$

which can be expressed more simply in terms of our polar co-ordinates as

$$u_x \sim f(x) \sin \theta / r.$$

At the next order we find a correction flow which near the drop is entirely in the  $yz$  plane with

$$u_r \sim -f' \sin \theta + f\eta'(1 + \cos 2\theta) / 2r,$$

$$u_\theta \sim -f\eta' \sin 2\theta / r.$$

A pressure disturbance is also generated near the drop to this order

$$p \sim -2\mu f' \sin \theta / r + 2\mu f\eta' \cos 2\theta / r^2.$$

The associated stress fields can now be calculated. At leading order we find

$$\sigma_{xr} = \sigma_{rx} \sim -\mu f \sin \theta / r^2, \quad \sigma_{x\theta} = \sigma_{\theta x} \sim \mu f \cos \theta / r^2.$$

Of the correction terms which occur at the next order, we shall only require

$$\sigma_{rr} \sim 2\mu f' \sin \theta / r - \mu f\eta'(1 + 3 \cos 2\theta) / r^2,$$

and

$$\sigma_{\theta r} \sim -\mu f' \cos \theta / r + \mu f\eta' \sin 2\theta / r^2.$$

At this same order care would be needed in calculating  $\sigma_{xx}$ , but the complications of the skewness of the co-ordinates can be avoided simply by differentiating the first expression for  $u_x$  which contains only Cartesian co-ordinates.

Examining the above expressions for the corrections to the velocity and stress, we see the need for an additional small disturbance flow  $O(f', f\eta')$  in the  $yz$  plane with a zero and a first harmonic variation in  $\theta$ . The components with the second harmonic variations will now be dropped because they would deform the cross-sectional shape of the drop which, as discussed in the introduction, we have assumed *ad hoc* to be circular. The required additional disturbance flow can then be generated by sources of strength  $2\pi g(s)$  and source-dipoles of strength  $2\pi h(s)$  distributed along the centre-line of the drop,

$$(u_x, u_y, u_z) = \int_{-l}^l \frac{1}{2}g(s) \frac{(x-s, y-\eta(s), z)}{[.]^{\frac{3}{2}}} + \frac{1}{2}h(s) \times \left[ \frac{(0, 1, 0)}{[.]^{\frac{3}{2}}} - \frac{3(y-\eta(s))(x-s, y-\eta(s), z)}{[.]^{\frac{5}{2}}} \right] ds,$$

in which  $[.] = (x-s)^2 + (y-\eta(s))^2 + z^2$ . This disturbance flow generates no pressure disturbance. Evaluating the integral asymptotically for the slender drop, we find that near the drop the flow is again entirely in the  $yz$  plane with

$$\begin{aligned} u_r &\sim g(x)/r + h(x) \sin \theta / r^2, \\ u_\theta &\sim -h(x) \cos \theta / r^2. \end{aligned}$$

There is no need to proceed beyond this leading order because  $g$  and  $h$  are small compared with  $f$ . The associated stress fields which we shall require are

$$\begin{aligned} \sigma_{rr} &\sim -2\mu g/r^2 - 4\mu h \sin \theta / r^3, \\ \sigma_{r\theta} &\sim 4\mu h \cos \theta / r^3. \end{aligned}$$

We now gather together the stress fields from the undisturbed flow and the distribution of stresslets, sources and dipoles to evaluate the boundary condition of continuity of surface stress. As in the previously studied cases of slender drop of low viscosity fluids (see, for example, Acrivos & Lo 1978), the stress inside the drop is dominated by a pressure  $p(x, t)$  which does not vary over the cross-section of the drop. Furthermore for a slender drop the curvature of the surface is asymptotically  $1/R$ , so with  $\gamma$  denoting the surface tension, the boundary condition on the stress is

$$\left(\frac{\gamma}{R} - p\right) \mathbf{n} = \boldsymbol{\sigma} \cdot \mathbf{n},$$

i.e.

$$\begin{aligned} \hat{\mathbf{r}} \left(\frac{\gamma}{R} - p\right) &= \hat{\mathbf{x}} \mu (E - f/R^2) \sin \theta \\ &+ \hat{\mathbf{r}} \mu \left\{ \frac{1}{2} \eta' (f/R^2 - E) - f\eta' / R^2 - 2g/R^2 + [R' (f/R^2 - E) + 2f'/R - 4h/R^3] \sin \theta \right\} \\ &+ \hat{\boldsymbol{\theta}} \mu \left\{ -R' (f/R^2 + E) - f'/R + 4h/R^3 \right\} \cos \theta. \end{aligned}$$

In the above, second harmonic terms have been left out for the reasons stated earlier, and correction terms  $o(\mu f/R^2)$  in the  $\hat{\mathbf{x}}$  direction and  $o(\mu f'/R^2, \mu f\eta'/R^2)$  in the  $\hat{\mathbf{r}}$  and  $\hat{\boldsymbol{\theta}}$  directions have been ignored as being small. The boundary condition is satisfied by choosing

$$f = ER^2, \quad h = ER^3R',$$

and

$$g = -(\gamma/R - p) R^2/2\mu - \frac{1}{2} ER^2\eta'.$$

With the flow outside the drop now known in terms of the shape and the internal pressure, we can obtain an equation for the evolution of the shape by applying the kinematic condition at the surface,

$$\begin{aligned} \dot{R} + \dot{\eta} \sin \theta &= \mathbf{u} \cdot \mathbf{n} \\ &= -E(R'\eta + \frac{1}{2}R\eta') + g/R + \sin \theta [-E(\eta\eta' + RR') - f' - fR'/R + h/R^2]. \end{aligned}$$

Substituting in the expressions for  $f$ ,  $g$  and  $h$ , we then arrive at

$$\begin{aligned} \dot{R} &= -E\eta R' - E\eta' R - \frac{\gamma}{2\mu} + \frac{p}{2\mu} R, \\ \dot{\eta} &= -E\eta\eta' - 3ERR'. \end{aligned}$$

It is worth remarking at this point that the same results can also be derived using the method of inner and outer expansions employed previously for the case of pure straining motion (Acrivos & Lo 1978; Hinch & Acrivos 1979). In contrast to those earlier studies, however, where the inner solution and the drop shape could be found to leading order without investigating the outer region, the inner solution to the present problem contains a function of  $x$  which can only be determined uniquely by matching with the outer solution. The method described above was therefore chosen for presentation since it requires only a single expansion for the solution which applies everywhere.

### 2.3. The internal flow

We complete the derivation of the governing equations by calculating the internal pressure distribution  $p(x, t)$ . The flow inside the slender drop is essentially that in a cylinder of radius  $R$  driven by a pressure gradient  $p'$  and an external velocity on the boundary  $u_x = E(\eta + R \sin \theta) + f \sin \theta / R$ . With  $\mu_i$  the internal viscosity, the flow inside the drop is thus

$$u_x = -\frac{R^2 - r^2}{4\mu_i} p' + E(\eta + 2r \sin \theta).$$

This flow produces a volume flux along the drop

$$q = -\frac{\pi R^4}{8\mu_i} p' + \pi R^2 \eta E,$$

and a divergence in the volume flux changes the radius in time according to

$$2\pi R \dot{R} + q' = 0.$$

Now on account of symmetry, there is no volume flux at the centre of the drop  $x = 0$ , so that integrating twice we find that

$$p = p_0(t) + 8\mu_i \int_0^x \left[ \frac{E\eta}{R^2} + \frac{2}{R^4} \int_0^x R \dot{R} dx \right] dx,$$

where the pressure at the centre of the drop  $p_0(t)$  has to be chosen so that the volume of the drop remains constant, i.e.

$$\int_{-l}^l \pi R^2 dx = \frac{4}{3} \pi a^3,$$

with  $a$  being the radius of a spherical drop having the same volume.

### 2.4. Non-dimensionalization

By combining the interior and exterior solutions, we obtain our equations of motion for the deformation of the drop. Letting  $\lambda \equiv \mu_i / \mu \ll 1$ , we non-dimensionalize these equations by scaling  $R$  and  $\eta$  with  $a\lambda^{\frac{1}{3}}$ ,  $x$  and  $l$  with  $a\lambda^{-\frac{1}{3}}$ ,  $t$  with  $E^{-1}\lambda^{-\frac{1}{2}}$  and  $p_0$  with  $\mu E \lambda^{\frac{1}{3}}$ . The non-dimensional equations are then

$$R = -\eta R' - \eta' R - \frac{1}{2G} + \frac{1}{2} p_0 R + 4R \int_0^x \left[ \frac{\eta}{R^2} + \frac{2}{R^4} \int_0^x R \dot{R} dx \right] dx,$$

$$\dot{\eta} = -\eta \eta' - 3R R',$$

together with the volume constraint

$$\int_0^l R^2 dx = \frac{2}{3}.$$

These are the governing equations which we shall use henceforth throughout the paper. We see that these equations contain just one non-dimensional parameter  $G = \lambda^{\frac{3}{2}} \mu E a / \gamma$ , the effective strength of the shear flow. The drop is slender as long as  $R/l \ll \lambda^{-\frac{1}{2}}$ .

Our governing equations were derived under the *ad hoc* approximation that the cross-section was circular. It is, therefore, important to examine the equations to see that each of the terms is physically reasonable and not just an undesirable artifact of our modelling. To begin with, we note that the first terms on the right-hand side of the  $\dot{R}$  and  $\dot{\eta}$  equations represent advection with the shear flow. Thus where the drop is above the plane of no flow,  $\eta > 0$ , the drop would expand,  $\dot{R} > 0$ , if it is fatter upstream,  $R' < 0$ , and fall,  $\dot{\eta} < 0$ , if it is lower upstream,  $\eta' > 0$ . The second term in the  $\dot{\eta}$  equation represents the need of a tapering drop,  $R' < 0$ , to rise,  $\dot{\eta} > 0$ , when the shear produces a velocity difference proportional to  $R$  across the drop; the drop must rise to ensure continuity of the normal velocity. The second term in the  $\dot{R}$  equation comes from the stretching,  $\dot{R} < 0$ , by the component of the strain-rate tensor along the centre-line of the drop when  $\eta' > 0$ . The third and the two final terms represent respectively the contraction of the drop,  $\dot{R} < 0$ , by the surface tension forces and its expansion,  $\dot{R} > 0$ , by pressure forces. We note that the pressure increases along the drop,  $p' > 0$ , when some return flow is required along its centre-line to cancel the flow along its surface, or to shorten its length ( $\dot{R} > 0$  for  $x$  small,  $\dot{R} < 0$  for  $x$  near  $l$ ). Thus the role of each of the terms in our governing equations can be accounted for in physical terms.

### 3. Equilibrium shapes

#### 3.1. The problem

The steady drop shapes can be determined by solving our governing equations with  $\dot{R}$  and  $\dot{\eta}$  set equal to zero. The  $\dot{\eta}$  equation can be integrated to give

$$\eta(x) = \pm [3(R^2(0) - R^2(x))]^{\frac{1}{2}},$$

where we take the positive root in  $x > 0$  and, on account of symmetry, the negative root in  $x < 0$ ; the other choice is unphysical and does not lead to a solution. Two immediate consequences of the above result are that the end of the drop at  $x = l$  is further up in the flow than the surface of the drop at the centre by a factor  $3^{\frac{1}{2}}$ , i.e.  $\eta(l) = 3^{\frac{1}{2}}R(0)$ , and that the upper surface of the drop has a displacement  $\eta + R$  with a maximum  $2R(0)$  which occurs when  $R = \frac{1}{2}R(0)$ .

When the above steady solution for  $\eta$  is substituted into the  $\dot{R}$  equation, we obtain the integro-differential equation for  $R$

$$-\frac{3^{\frac{1}{2}}(R^2(0) - 2R^2)}{(R^2(0) - R^2)^{\frac{3}{2}}} R' - \frac{1}{2G} + \frac{1}{2}p_0 R + 3^{\frac{1}{2}}4R \int_0^x \frac{(R^2(0) - R^2)^{\frac{1}{2}}}{R^2} dx = 0.$$

This equation is mildly singular at  $R = 0$  and  $R(0)$ , and strongly singular at  $R = R(0)/2^{\frac{1}{2}}$ . The latter singularity can and must be avoided by choosing  $p_0$ , the pressure at the centre, so that at the singularity the pressure is  $2^{\frac{1}{2}}/GR(0)$ . It is interesting to contrast this requirement in simple shear flow that  $p_0$  must be uniquely chosen with

the corresponding non-uniqueness found in pure straining flows. Specifically, for the case of an axisymmetric straining motion, Buckmaster (1972, 1973), was the first to observe that any pressure at the centre gave an equilibrium shape, although only a countably infinite set gave shapes which were smooth analytic functions at the origin. The selection of a unique realizable equilibrium shape from this discrete set was finally made by Acrivos & Lo (1978) from a stability analysis. The key difference between the extensional and shear flows is that the component of the strain-rate tensor along the centre-line of the drop,  $\eta'$ , (in the  $-\eta'R$  term of the  $\dot{R}$  equation) varies in our shear flow, decreasing to zero at the end, whereas the corresponding term in the extensional flow is constant. Of even more importance though is the fact that this component of the strain rate,  $\eta'$ , as well as depending on  $R$ , is directly proportional to the tapering of the drop,  $R'$ , so that the combined effect of the advection and stretching terms  $-\eta R' - \eta'R$  in the  $R$  equation is proportional to  $R'$ . Thus, near the middle, the drop has a tendency proportional to  $R'$  to contract through stretching; and at the ends it has a tendency proportional to  $R'$  to expand through advection. Thus unless the pressure and surface tension terms cancel each other at the point where these tendencies become equal (with the expanding pressure dominating into the middle and the contracting surface tension dominating at the ends), the tapering  $R'$  has to become infinite to achieve a balance.

To solve the above equation for the equilibrium shape of the drop, a rescaling of the radius and length proves convenient. To this end we set  $x = 3^{\frac{1}{2}}2GR^2(0)z$ ,  $R(x) = R(0)F(z)$  and  $p = P_0/GR(0)$ . The equation then becomes

$$\frac{1 - 2F^2}{(1 - F^2)^{\frac{1}{2}}} \frac{dF}{dz} + 1 - P_0 F - \alpha F \int_1^F \frac{(1 - F^2)^{\frac{1}{2}} dz}{F^2} dF = 0,$$

in which the parameter  $\alpha = 48G^2R^2(0)$ . The problem has now been reduced to the following. A value of  $\alpha$  is selected and the integro-differential equation is solved with the constant  $P_0$  chosen to avoid the singularity at  $F = 2^{-\frac{1}{2}}$ . Then  $R(0)$  and  $G$  are calculated from the value of  $\alpha$  and the volume normalization

$$-3^{\frac{1}{2}}2GR^4(0) \int_0^1 F^2 \frac{dz}{dF} dF = \frac{2}{3}.$$

Finally the dimensionless half-length of the drop is found as  $l = 3^{\frac{1}{2}}2GR^2(0)z_1$ , where  $z_1$  is the first root of  $F(z) = 0$ .

### 3.2. $G$ small

The limit of small  $\alpha$  can be solved analytically. This limit which ignores the variation of the pressure inside the drop corresponds to an inviscid drop or equivalently low shear rates because making  $\lambda$  small also reduces  $G$ . The differential equation can be integrated directly taking  $P_0 = 2^{\frac{1}{2}}$  to produce an implicit expression for the shape

$$z = \cos^{-1} F + 2^{\frac{1}{2}}(1 - F^2)^{\frac{1}{2}},$$

which when substituted in the volume constraint yields

$$R^4(0) = (24)^{-\frac{1}{2}}(1 + 3\pi/2^{\frac{1}{2}}8)^{-1}G^{-1}.$$

Finally the relation between the dimensionless half-length of the drop and the shear rate is found to be

$$l = 3.45G^{\frac{1}{2}},$$

from which it is apparent that the dimensional length does not depend on the value of  $\mu_i$ , clearly an appropriate result for an inviscid drop  $\mu_i = 0$ . The  $G$  dependence of the length at low shear rates should be contrasted with the  $(\mu a E / \gamma)^2$  dependence of low strain rates in pure straining motions. The drop in simple shear is longer because the component of the strain rate along the centre-line of the droplet is not  $O(1)$  as in extensional flows but, as already mentioned in the introduction, is  $O(R/l)$  which also equals  $O(l^{-\frac{3}{2}})$  from the volume normalization condition. Balancing the strain rate with the surface tension term  $O(G^{-1}R^{-1}) = O(G^{-1}l^{\frac{1}{2}})$ , yields then  $l = O(G^{\frac{1}{2}})$  in simple shear and  $l = O(G^2)$  in pure extension. To keep the drop slender when  $G$  is small we need the dimensional aspect ratio  $\lambda^{\frac{1}{2}}R(0)/l = 0.227\lambda^{\frac{1}{2}}G^{-\frac{3}{2}}$  small.

### 3.3. An approximate solution

An approximate way of solving the integro-differential equation for  $F$  when  $\alpha$  is not small is to replace the integral by its form in the middle of the drop, i.e. by  $(1-F)/(P_0-1)$ . This approximation, which relies on the central part of the drop dominating the dynamics, was successfully used in the corresponding problem in axisymmetric extensional flow by Acrivos & Lo (1978) who computed a critical shear rate within 2% of the exact value. When the same approximation is made here and the pressure  $P_0$  is chosen so as to remove the singularity at  $F = 2^{-\frac{1}{2}}$ , we find that

$$P_0 = \frac{1}{2}\{2^{\frac{1}{2}} + 1 \pm (2^{\frac{1}{2}} - 1)[1 - 2^{\frac{1}{2}}\alpha/(2^{\frac{1}{2}} - 1)]^{\frac{1}{2}}\},$$

and that the integro-differential equation reduces to

$$\frac{1 + 2^{\frac{1}{2}}F}{(1-F^2)^{\frac{1}{2}}} \frac{dF}{dz} + 1 - AF = 0,$$

where  $A = (2^{\frac{1}{2}} - P_0)/(2^{\frac{1}{2}} - 1)$ . This can be integrated to give for the volume normalization

$$3^{\frac{1}{2}}2GR^4(0) \left[ \left(1 + \frac{2^{\frac{1}{2}}}{A}\right) \frac{B}{A^2} - \frac{\pi}{2^{\frac{1}{2}}A^2} - \frac{1}{A^2} \left(1 + \frac{\pi}{2^{\frac{1}{2}}}\right) (2^{\frac{1}{2}} + A) \right] = \frac{2}{3},$$

and for the scaled length

$$z_1 = \left(1 + \frac{2^{\frac{1}{2}}}{A}\right) B - \frac{\pi}{2^{\frac{1}{2}}A},$$

in which  $B = [2/(1-A^2)^{\frac{1}{2}}] \tan^{-1}[(1+A)/(1-A)]^{\frac{1}{2}}$ . The results from this approximate solution are plotted in figure 2. It is seen that the shape of this approximate deformation curve is qualitatively similar to that found by Acrivos & Lo (1978) in extensional flow and this suggests that the internal pressure gradient has a similar effect in both cases. Specifically, the lower internal pressure at the middle compared with that at the ends (required to drive a return flow along the centre portion of the drop) reduces the tapering at the middle and so leads to a longer drop than one with a constant internal pressure. The effect increases with  $G$ , because the pressure difference between

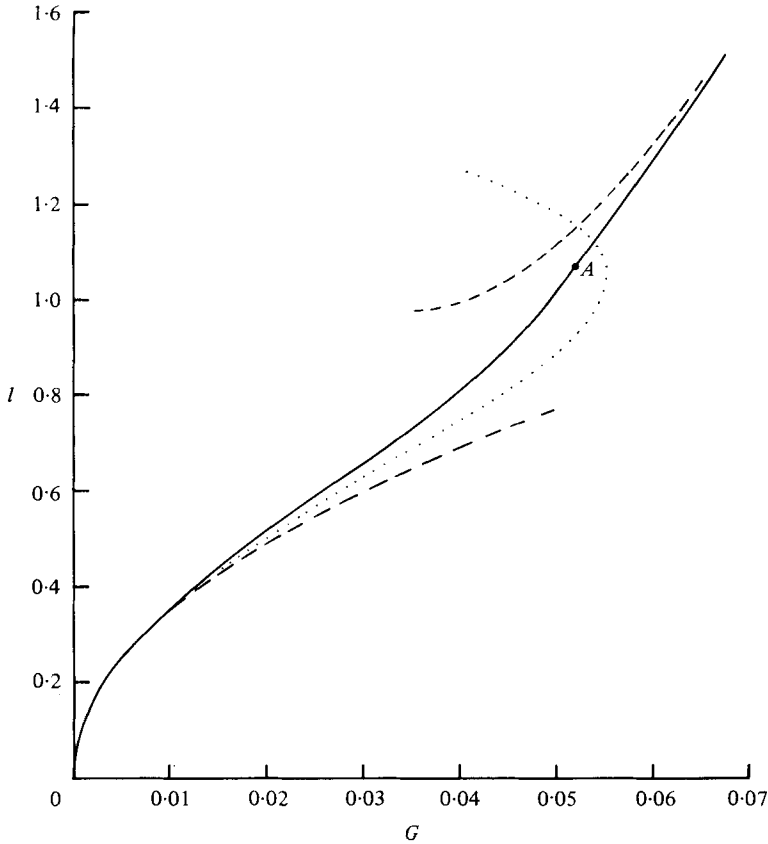


FIGURE 2. The dimensionless half-length of the equilibrium drop as a function of the shear rate. The solid curve is the numerical result from §§ 3.4 and 3.5, with the point  $A$  corresponding to  $\alpha = 0.125$ . The dashed curves are the asymptotes for  $G \rightarrow 0$  from § 3.2 and for  $G \rightarrow \infty$  from § 3.6, while the dotted curve is the prediction of the approximate solution of § 3.3.

the middle and the ends increases as the length increases. At a shear rate of  $G = 0.0549$ , the approximate solution suggests that a critical state is reached from which further increases in length reduce the pressure at the centre more than they reduce the tapering, and so no equilibrium shape can exist beyond this shear rate. By the same argument the upper branch of the solutions produced by the approximate solution would be unstable.

### 3.4. An iterative numerical method

The small  $\alpha$  solution and the approximate solution suggest a numerical scheme for solving the integro-differential equation for  $F(z)$ . We take  $F$  to be the dependent and  $z$  the independent variables. Then the equation is used iteratively to find  $(1 - F^2)^{1/2} dz/dF$ , substituting the current form into the integral to find the next iterate. The integral was computed by the trapezoidal rule after the singular terms in the integrand proportional to  $F^{-2}$  and  $F^{-1}$  as  $F \rightarrow 0$  had been subtracted and evaluated analytically. Better than 4 figure accuracy was achieved with 10 equally spaced points in the range of integration. At each stage of the iteration the pressure  $P_0$  was determined by requiring that no singularity should exist at  $F = 2^{-1/2}$  in the next iterate. A suitable

test for the convergence of the iteration was found to be that  $(1-F^2)^{\frac{1}{2}}dz/dF$  at  $F = 1$  changed by less than  $10^{-4}$ . For  $\alpha < 0.1$  the iteration converged within 10 steps starting from the null function, but at larger  $\alpha$  it proved much faster to start the iteration from the converged result for a nearby  $\alpha$ . No convergence could be achieved for  $\alpha > 0.125$ . From the converged results for  $(1-F^2)^{\frac{1}{2}}dz/dF$ , the volume normalization integral and the integral for the scaled length  $z_1 = \int_0^1 (dz/dF) dF$  were evaluated after subtracting off the  $(1-F^2)^{-\frac{1}{2}}$  behaviour at  $F \rightarrow 1$  and integrating that part analytically.

The results from the iterative numerical scheme are plotted in figure 2 as the solid curve from the origin to the point  $A$  where  $\alpha = 0.125$ . Also shown are the deformation curve from the approximate solution of § 3.3 and the asymptote for small  $G$  from § 3.2. Clearly the numerical results do not exhibit the doubling back of the approximate solution at  $G = 0.0549$ , although up to  $G = 0.05$  the two solutions are within 10% of each other. On the other hand the asymptotic expression for small  $G$  deviates from the exact solution by more than 10% when  $G > 0.03$  and is in error by more than 25% when  $G = 0.05$ . Therefore from a practical point of view the approximate solution has some merit.

### 3.5. A second numerical scheme

The fact that the results from the iterative numerical scheme end abruptly at the point  $A$  in figure 2 ( $\alpha = 0.125$ ) hints at a numerical failure and not a physical one. An alternative numerical scheme was therefore devised which did indeed yield solutions for higher shear rates and these are plotted in figure 2 beyond the point  $A$ . This scheme replaced the integro-differential equation for  $F$  by two coupled differential equations

$$\frac{dF}{dz} = \frac{(1-F^2)^{\frac{1}{2}}(PF-1)}{1-2F^2},$$

$$\frac{dP}{dz} = \alpha \frac{(1-F^2)^{\frac{1}{2}}}{F^2},$$

which were solved by a fourth-order Runge-Kutta procedure. The singularity at  $F = 2^{-\frac{1}{2}}$  was removed by starting the integrations at  $F = 2^{-\frac{1}{2}}$  with  $P = 2^{\frac{1}{2}}$ . Because the expression for  $dF/dz$  is indeterminate at this point, a local analysis is necessary which yields  $dF/dz = -\frac{1}{2}[2^{-\frac{3}{2}} \pm (\frac{1}{8} - \alpha)^{\frac{1}{2}}]$  at  $F = 2^{-\frac{1}{2}}$ . This result shows why the iterative scheme failed when  $\alpha > 0.125$ . Starting with one of the two choices for  $dF/dz$  at  $F = 2^{-\frac{1}{2}}$ , the differential equations were integrated first forwards to  $F = 0$  and then backwards to  $F = 1$ . The singular points at  $F = 0$  and  $F = 1$  were avoided by extrapolating from  $F$  and  $dF/dz$  to anticipate the position of the end and of the centre and then stopping the integration three steps ahead of the singularity. The extrapolations  $F \sim 1 - kz^2$  as  $z \rightarrow 0$  and  $F \sim [\frac{1}{2} + (\frac{1}{4} - \alpha)^{\frac{1}{2}}](z_1 - z) \times (1 - k(z - z_1)^{0.75})$  as  $z \rightarrow z_1$  were employed, in which  $k$  is unknown and the exponent 0.75 is arbitrary but successful. Simultaneously with the evaluation of  $F$  from the differential equations,  $F^2$  was integrated for use in the volume normalization condition and extrapolations similar to the above were made to  $F = 0$  and 1. A step size of 0.05 was found necessary to give 4 figure accuracy in  $z_1$  and  $\int_0^1 F^2 dz$ , the error mainly coming from poor extrapolations.

The results of this second numerical scheme are plotted in figure 2 in the solid curve. Of the two choices for  $dF/dz$  at  $F = 2^{-\frac{1}{2}}$ , the positive root yields the curve from the origin to the point  $A$  as  $\alpha$  increases from 0 to 0.125 and the negative root the curve from the point  $A$  onwards as  $\alpha$  decreases from 0.125 to 0.12262 where  $G$  becomes infinite. The duplication of the numerical results up to the point  $A$  by a totally different method serves as a useful check. The additional results beyond the point  $A$  show that an equilibrium shape for the drop exists for all shear rates. This behaviour should be contrasted with the corresponding solution of the extensional flow problem as well as the prediction of our approximate solution in § 3.3, according to which equilibrium shapes can exist only up to some critical shear rate.

### 3.6. $G$ large

The numerical results show that as  $G \rightarrow \infty$  the drop takes a special form. A long central part of length  $261G^2$  has a constant radius  $R = 0.0505/G$  and is fully aligned with the flow. In this central part the pressure and surface tension forces are in exact balance, an equilibrium which looks suspiciously unstable. At the ends of the drop there are small regions of length  $O(G^{-1})$  in which the drop tapers and the centre-line rises. As  $G \rightarrow \infty$  the end regions tend to a constant shape with a size proportional to  $G^{-1}$ . Also all the dynamical effects in the  $R$  equation play a role only in the end regions. Our earlier approximation clearly fails therefore because it was designed to model the central part of the drop and represents the important end regions rather poorly. As a consequence of the fact that the radius remains constant in the long central part ( $F = 1$ ), we can evaluate asymptotically the integral in the volume normalization condition

$$\int_0^{z_1} F^2 dz \sim z_1 - 2.61,$$

in which the correction 2.61 for the ends has been extracted from the numerical solutions. This result together with  $\alpha \rightarrow 0.12262$  yield the asymptotic estimate for the length of the drop at high shear rates

$$l \sim 261G^2 + 0.0231/G \quad \text{as } G \rightarrow \infty,$$

which lies within 10 % of the numerical solution for  $G > 0.05$ .

The asymptotic form of the equilibrium shape as  $G \rightarrow \infty$  explains why equilibria exist at high flow rates in shear flow but not in extensional flows. As we have explained earlier, very long drops cannot exist in extensional flows because it proves impossible to support the pressure difference within the drop between its ends and its middle which is required in order that the fluid dragged along by the external flow be returned along the axis of the drop. But in shear flow the long drops avoid the need for a large internal pressure difference by aligning themselves very closely with the flow. In such an orientation, a pressure induced return flow is not required because the flux of fluid dragged along by the top surface is cancelled by an opposite flux from the bottom surface.

#### 4. Time dependent motions

##### 4.1. *The numerical method*

Our prediction of equilibria at all shear rates conflicts with the experimental observation of drops breaking up when the shear rate is too high. This conflict and the cylindrical form of the computed steady shapes at high shear rates lead us to study the stability of our equilibria. As a linear stability analysis generates a difficult numerical problem, we chose to solve numerically the full governing equations of § 2.4 as an initial value problem. Moreover this numerical approach allowed us to investigate some interesting nonlinear motions which will be discussed in § 4.5.

Our attempts to set up a finite difference scheme for the problem proved unsuccessful. The changing length of the drop in time can be handled with no difficulty by adding and subtracting extra points as required, or by recasting the equations in terms of  $x/l(t)$ . The trouble with the problem is that the governing equations are hyperbolic and the advection plays an important role. Several explicit schemes were tried but all were unstable being unable to handle the varying advection velocity. Application of the method of characteristics was considered, but this proved unattractive owing to a continuous loss of characteristics through the ends which require new ones to be added in a long time run, and the fact that the ends were located at the difficult points where the characteristics become parallel.

An alternative numerical approach is to represent the shape by a linear combination of modal functions with the combination able to change in time. We chose to represent the shape as a simple polynomial of  $x$  with time dependent coefficients. The powers of  $x$  have the advantage that they can be manipulated more simply in this nonlinear problem than other modal functions, and they are well suited to represent the monotonic functions  $R$  and  $\eta$  which if anything require slightly more flexibility at the ends. We call the representation

$$\begin{aligned} R(x, t) &\approx R_0(t) + R_1(t)x^2 + \dots + R_N(t)x^{2N}, \\ \eta(x, t) &\approx \eta_0(t)x + \dots + \eta_{N-1}(t)x^{2N-1}, \end{aligned}$$

an  $N$ -term representation. It was found convenient to use a polynomial for  $\eta$  of one degree lower than that for  $R$ , although the extra  $\eta_N(t)x^{2N+1}$  term in  $\eta$  was added occasionally and sometimes it gave more accurate results.

Our numerical scheme was to substitute an  $N$ -term representation into the right hand side of the governing equations of § 2.4 expand in powers of  $x$ , and then read off the coefficient of  $x$  on the right hand side as  $\dot{R}_n$  or  $\dot{\eta}_n$ . The program had to be able to multiply and divide two polynomials, retaining terms up to  $x^{2N}$ . Two key steps are the treatment of the pressure and the handling of the integral involving the unknown  $\dot{R}$ . The latter problem was solved by our particular representation of  $R(x, t)$ , because in calculating the coefficient of  $x^{2n}$  from the integral, one only needs to know  $\dot{R}_m$ ,  $m < n$ , and hence  $\dot{R}$  can be generated inductively starting from  $\dot{R}_0$  and ending at  $\dot{R}_N$ . The pressure  $p_0$  has to be chosen to preserve the volume, i.e. so that

$$\int_0^l R \dot{R} dx = 0.$$

To choose the correct value we exploit the linearity of  $\dot{R}$  in  $p_0$ . Thus, we evaluate  $\dot{R}$

first for  $p_0 = 0$  and then for  $p_0 = 1$  and find which linear combination of the two makes the integral vanish. When evaluating the integral it is important to multiply the polynomials for  $R$  and  $\dot{R}$  exactly, and not to truncate the product after  $x^{2N}$ . The length  $l$ , which is needed in the integration, is found from the value at a previous time step by a Newton–Raphson method, with  $R'(l)$  readily evaluated from the polynomial representation. A single iteration on the length was always found to be sufficient.

The values for the time derivatives  $\dot{R}_n$  and  $\dot{\eta}_n$  were used to step the shape of the drop forward in time with a fourth order Runge–Kutta method. Four figure accuracy could generally be obtained with a time step of 0.05 for  $N = 4$ , 0.025 for  $N = 7$  and 0.01 for  $N = 10$ . At very low values of  $G$  and whenever certain rapid motions occurred, smaller time steps were necessary. Although the numerical scheme is designed to preserve the polynomial representation of the volume, there was some small drift over a long time. This drift is equivalent to changing  $G$  slightly, which we shall see is significant in some circumstances. We therefore renormalized the volume at regular intervals by multiplying both the  $R_n$  and  $\eta_n$  terms by the factor necessary to restore the volume.

Some checks on the complicated program are essential. There are the internal checks that the volume is almost preserved without the renormalizations and that the accuracy improves in a certain way with smaller time steps. In the special cases  $N = 1$  and 2 the values of  $\dot{R}_n$  and  $\dot{\eta}_n$  were compared with those obtained from separately derived expressions. Finally, predictions of the equilibrium shape of the drop were compared with those obtained in § 3, as we shall report in § 4.3.

#### 4.2. A simple model

The special case  $N = 1$  provides a simple model of the motions of the drop and we shall turn to it at several points in this section. In this model, the radius of the drop has a quadratic variation while the centre-line is straight with a time-dependent slope. Clearly the model cannot be expected to represent accurately the high  $G$  equilibria.

Now owing to the volume constraint, one of the two variables  $R_0$  and  $R_1$  can be eliminated, so that the model is governed by a second-order system of ordinary differential equations. Actually, instead of the original variables  $\eta_0$  plus either  $R_0$  or  $R_1$ , it is more convenient to use two related variables, the length  $l$  and the height of the end  $h = \eta(l) = \eta_0 l$ , in terms of which the governing equations for our  $N = 1$  model become

$$\dot{l} = h - \frac{1}{5^{1/2} 2G} \frac{l^{3/2}}{1 + 0.8l^3},$$

$$\dot{h} = \frac{1}{2} l^{-2} - \frac{1}{5^{1/2} 2G} \frac{hl^{1/2}}{1 + 0.8l^3}.$$

The first term in the  $\dot{l}$  equation represents the lengthening of the drop through advection, while the second represents contraction due to surface tension. The growing differences in internal pressure between the ends and the middle reduce the efficiency of the surface tension as the length becomes large. Moreover, the height of the end of the drop rises according to the first term in the  $\dot{h}$  equation owing to the velocity difference over the cross section of a tapering drop, and sinks according to the second term as surface tension reduces the length. The effect on  $h$  of the advection increasing

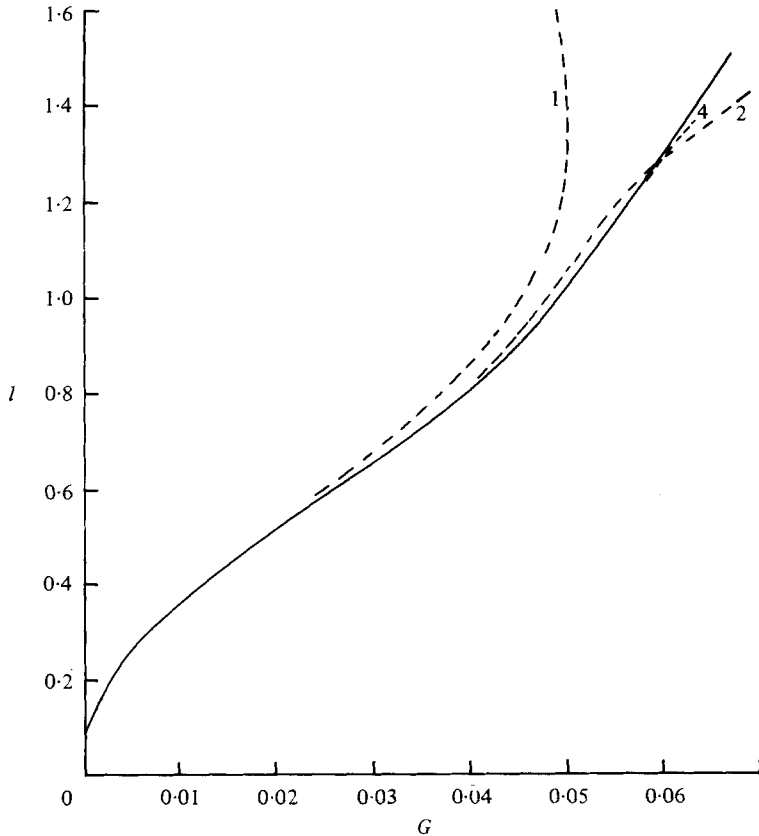


FIGURE 3. The dimensionless half-length of the equilibrium drop as a function of the shear rate. The solid curve is the numerical result of § 3, and the dashed curves are the predictions of the 1-term, 2-term and 4-term polynomial representations.

the length precisely cancels the effect of the advection on decreasing the height of the end on an upward sloping centre-line (as with the  $-\eta\eta'$  term in the original  $\eta$  equation in § 2.4).

#### 4.3. *The equilibrium shapes*

As a check on the suitability of the polynomial representation and to guard against errors in programming, the governing equations were integrated until an equilibrium shape was attained which could then be compared with the results of § 3. At low rates of shear,  $G < 0.04$ , an initial shape  $R = (5/4l)^{1/2}(1 - x^2/l^2)$ ,  $\eta = (15/4l^3)^{1/2}x$  was used with a reasonable guess for the length  $l$ . At higher shear rates it proved necessary to start from the equilibrium corresponding to a nearby shear rate. The equilibrium was found to be unstable for  $G = 0.054$ , see § 4.4, and so could not be reached by solving the initial value problem. We found that the instability could be deferred up to shear rates beyond those of interest by the artificial device of replacing the  $\dot{\eta}_n$  equations by the expressions for  $\eta_n$  in terms of  $R_m$ ,  $0 \leq m \leq n+1$ , which give  $\dot{\eta}_n \equiv 0$ , and then finding the equilibrium by solving the initial value problem for the restricted problem in which only the  $R_n$  vary freely.

Figure 3 depicts the dimensionless half-length of the steady-state drop as a function of shear rate, the solid curve being the results of § 3 already presented, while the dashed curves are for the  $N$ -term representations. Our simple model of § 4.2, the 1-term representation, has an equilibrium dimensionless half-length given implicitly by

$$G = \frac{1}{6\frac{1}{2}5} \frac{l^2}{1 + 0.8l^3}.$$

At low shear rates  $l \sim 3.50G^{\frac{1}{2}}$  for the 1-term representation instead of  $3.45G^{\frac{1}{2}}$  found in § 3.2. As seen in figure 3, below the critical shear rate  $G = 0.0501$  the 1-term representation has two equilibria, one with a length greater and one with a length less than 1.357, while above the critical shear rate there are no equilibria. The 1-term representation predicts the length to within 10% up to  $G = 0.045$ . The 2-term representation, which does not show the doubling back of the 1-term representation, predicts the length more accurately, keeping within 3% up to  $G = 0.062$  and becoming 10% off by  $G = 0.07$ . The addition of further terms slowly improves the accuracy particularly below  $G = 0.06$ .

A more critical test for the polynomial representation is the height of the end of the equilibrium drop  $\eta(l)$ . The results for the reciprocal of this quantity are shown in figure 4. Our simple model, the 1-term representation, is 45% off in its prediction of the height of the end by  $G = 0.045$ , while the 2-term representation is 23% off. To achieve a 5% accuracy at  $G = 0.045$  5 terms are necessary, while to maintain this accuracy to  $G = 0.06$  10 terms are required.

The height of the end of the steady-state drop is predicted more accurately if the extra  $\eta_N x^{2N+1}$  term is added to the  $N$ -term representation of  $\eta$ , although these augmented representations predict the length of the drop less accurately. Thus at  $G = 0.045$  the augmented 2-term representation predicts the length with a 5% error and the height of the end with a 0.3% error, while at  $G = 0.06$  the augmented 10-term representation predicts the length with a 3% error and the height of the end with a 0.7% error.

The shape of the equilibrium drop at  $G = 0.055$  is given in figure 5 where we have plotted the height of the upper and lower surfaces,  $y = \eta \pm R$ , as a function of  $x$ . Again the solid curve was obtained by the numerical method of § 3.5 with  $\alpha = 0.1243$ . The polynomial representations are poorest at the tip, 7 terms being needed for 6% accuracy and 10 terms for a 3% accuracy.

We conclude therefore from this study of equilibrium drops that the polynomial representation works well for  $G < 0.06$  with about 10 terms.

#### 4.4. The linear stability of the equilibrium

As just noted, the equilibrium cannot be found by solving the initial value problem for  $G > 0.054$  because the equilibrium is unstable. The stability was further investigated by solving the initial value problem starting very near to the equilibrium. A suitable perturbation to the equilibrium was made by rounding off the equilibrium values of the  $R_n$  and  $\eta_n$  usually to two significant figures. The drop was found to oscillate in time about the equilibrium, the oscillation decaying for  $G < 0.054$  and increasing for  $G > 0.054$ . While the oscillation remained small compared with the equilibrium but large compared with numerical noise, the oscillation settled down in one cycle to a single exponentially decaying or growing sinusoidal oscillation. The

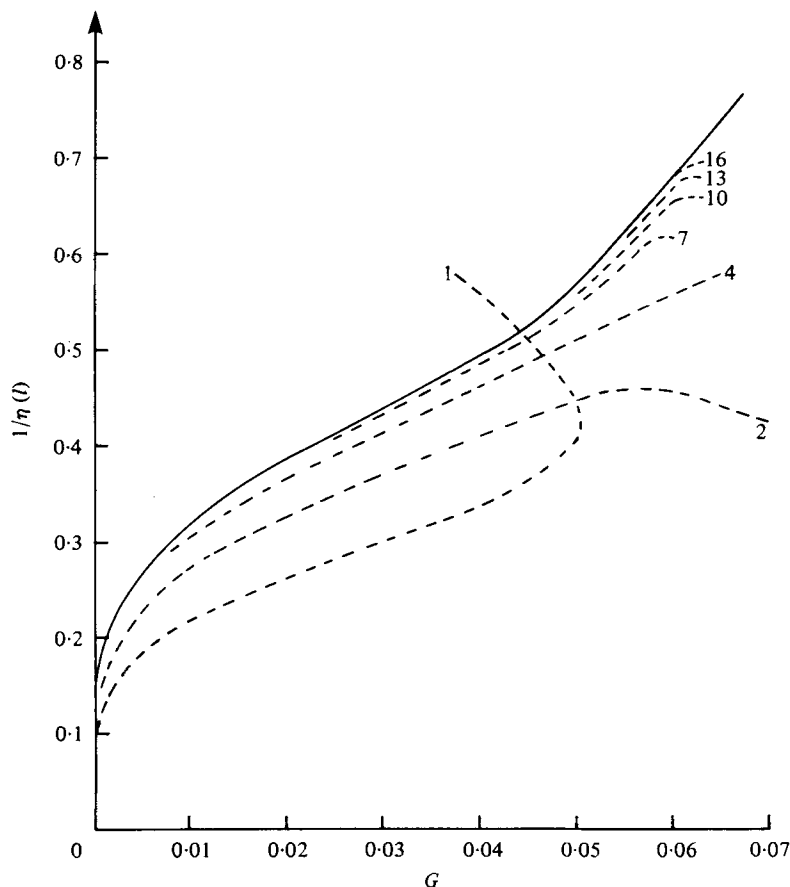


FIGURE 4. The reciprocal of the height of the end of the equilibrium drop as a function of the shear rate. The solid curve is the numerical result of § 3 and the dashed curves the predictions of the polynomial representations.

frequency of the oscillation  $\omega_r$  and the exponential decay rate  $\omega_i$  were extracted from the minima and maxima of the oscillations in the length and height of the end,  $\eta(l)$ . This method of analysing the data seemed to have an inherent inaccuracy of 2%, and failed to give sensible results when  $G < 0.02$  because the oscillation decayed too rapidly, and failed when  $G > 0.055$  because the oscillation grew too fast.

Figure 6 gives the results for the frequency and decay rate for this lowest mode of small amplitude disturbances. The solid curve was obtained with a 10-term representation, a 7-term representation producing results which differed by 2%, the inherent error of the data analysis. A quadratic interpolation through the results for  $G = 0.05$ ,  $0.0525$  and  $0.055$  finds that the decay rate becomes negative at  $G = 0.0541$ . Thus the equilibrium shape is unstable to small disturbances for  $G > 0.0541$ .

The dashed curve in figure 6 gives the results from our simple model, the 1-term representation, for the frequency  $\omega_r$  and the decay rate  $\omega_i$ ,

$$\omega_i + i\omega_r = \left(\frac{15}{27^3}\right)^{\frac{1}{2}} \left[1 + \frac{1}{4}\chi \pm i\left(2 + \frac{1}{2}\chi - \frac{1}{16}\chi^2\right)^{\frac{1}{2}}\right],$$

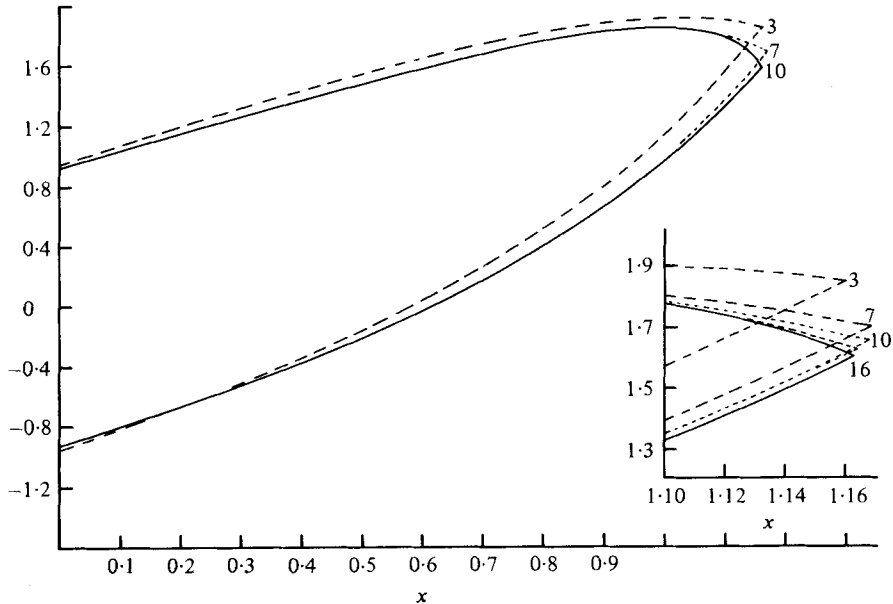


FIGURE 5. The shape of the equilibrium drop at  $G = 0.055$ . The solid curve is the numerical result of § 3 and the dashed curves the predictions of the polynomial representations.

in which  $\chi = (1 - 4l^3)/(1 + 0.8l^3)$ , with  $l$  the dimensionless half-length of the equilibrium drop. These predictions are within 23% of the results with the 10-term representation for  $G < 0.035$ . The model further suggests that as  $G \rightarrow 0$  the frequency and the decay rate should scale with  $G^{-\frac{1}{2}}$  with a correction term  $O(G^{\frac{1}{2}})$ . An analysis of the results for the 10-term representation does yield  $\omega_r \sim 0.619G^{-\frac{1}{2}} - 35.2G^{\frac{1}{2}}$  and  $\omega_i \sim 0.577G^{-\frac{1}{2}} - 47.4G^{\frac{1}{2}}$  as  $G \rightarrow 0$ . The leading order terms are 30% off by  $G = 0.02$ , but with the correction terms the asymptotic forms stay within 10% until  $G = 0.045$ . The  $G^{\frac{1}{2}}$  time scale for  $G \rightarrow 0$  is the time in which the surface tension  $G^{-1}$  changes the radius  $G^{-\frac{1}{2}}$  significantly, the radius  $G^{-\frac{1}{2}}$  corresponding to the length  $G^{\frac{1}{2}}$  from § 3.2 and the volume constraint.

The origin of the oscillation about the equilibrium can be found in the combination of a rotation of the drop which depends on its length and a stretching of the drop which depends on its orientation. In the discussion of the  $\eta$  equation at the end of § 2.4, we noted that the drop tends to sink,  $\dot{\eta} < 0$ , due to advection (if  $\eta\eta' > 0$ ) and rise,  $\dot{\eta} > 0$ , due to the tapering of the droplet (if  $RR' < 0$ ). Thus, relative to the equilibrium, we would expect a shorter drop with a larger radius and tapering to rise, while a longer one would correspondingly sink. On the other hand the length of the drop is determined by the balance of stretching by the flow with shrinking by surface tension. Thus when a drop is higher in the flow than the equilibrium it feels larger velocities and so is stretched, while a drop lower than when in equilibrium would correspondingly shrink. Combining the effects of the rotation and stretching we produce an oscillation: relative to the equilibrium a longer drop sinks, a lower drop contracts, a shorter drop rises, and a higher drop extends. A similar oscillation about the equilibrium is found in nearly spherical drops in a weak shear flow, Cox (1969).

The above description of the oscillation says nothing about the stability of the

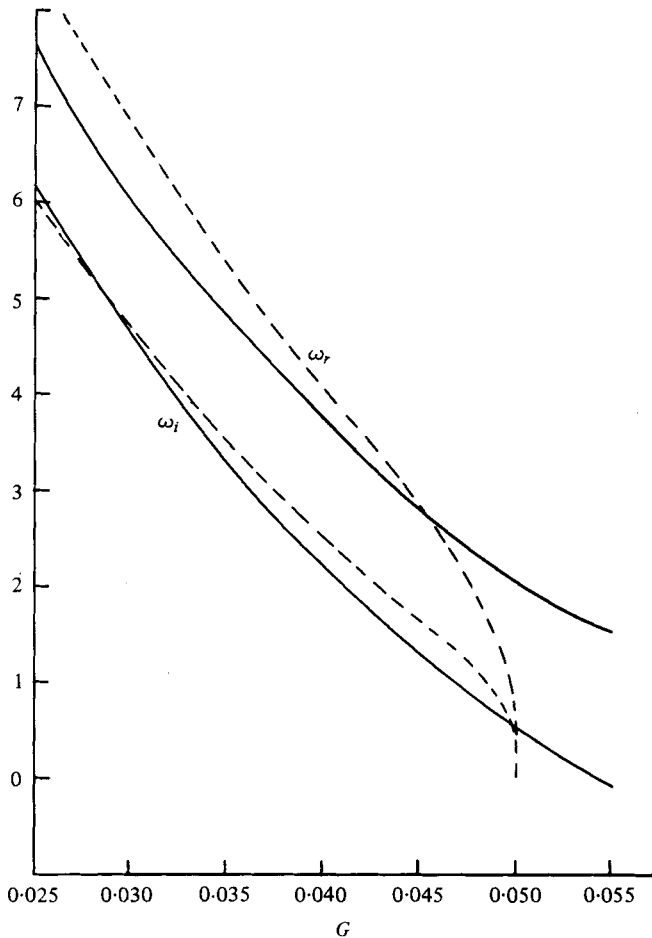


FIGURE 6. The frequency  $\omega_r$  and the exponential decay rate  $\omega_i$  of the lowest mode of small disturbances as a function of the shear rate. The dashed curves are for the  $N = 1$  model.

equilibrium. The decay of the oscillation comes from another effect: the tendency of the drop to return to its equilibrium length when the drop is in the equilibrium orientation. It appears that the internal pressure differences, which increase rapidly with the length of the drop for a given orientation, destroy the stability of an equilibrium if the dimensionless half-length exceeds 1.13 by the same mechanism that operates in pure straining flows on drops exceeding a non-dimensional half-length 0.63. The principal difference between the behaviour of drops in simple shearing and in pure straining flows is that the internal pressure differences do not preclude the existence of equilibria above a critical shear rate because the drop can assume an orientation in which it feels very little straining.

We note that the least stable mode of disturbance of the drop is found to have a length scale of the length of the drop, i.e. the maximum permitted wavelength. This result for the linear stability of a finite length drop is different from that for an infinitely long cylindrical drop, which has a least stable mode with a wavelength comparable to the thickness. The difference is due to the finite length drop having an equilibrium with a stabilizing curvature which must be overcome by a disturbance of finite

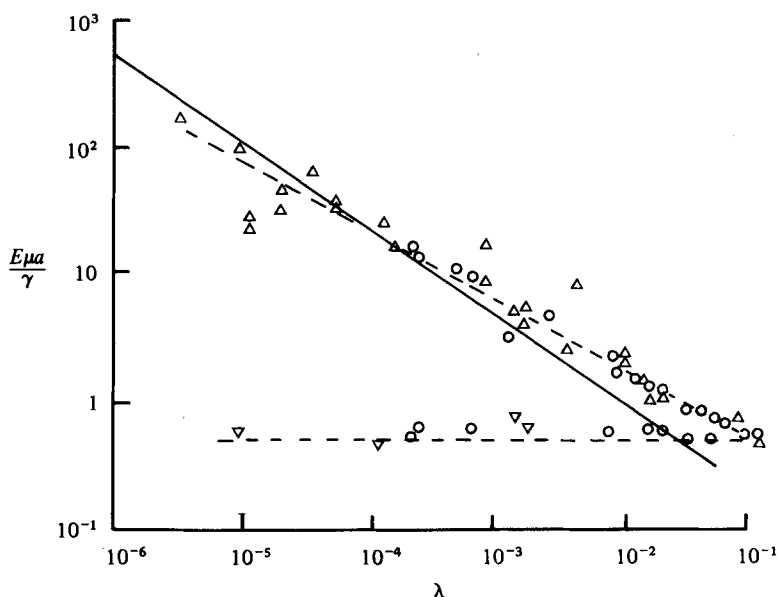


FIGURE 7. Comparison between the theoretical prediction and Grace's (1971) observation of the critical shear rate for break up as a function of the viscosity ratio:  $\circ$ , 45.5 P;  $\triangle$ , 502 P;  $\nabla$ , 2815 P. The solid curve gives the theoretical prediction  $E\mu a/\gamma = 0.0541 \lambda^{-2/3}$ , while the dashed curves are the best fits through the experimental observations of the break-up due to fracture  $E\mu a/\gamma = 0.17 \lambda^{-0.55}$  and the break-up due to tip streaming  $E\mu a/\gamma = 0.56$ .

amplitude. The fact that the wavelength of greatest interest is long is fortunate because we can only study long wavelength disturbances with our slender drop equations. Furthermore, cross-sectional shape disturbances, which of course we cannot study with our present analysis, should be similar to short wavelength disturbances and of little interest.

We compare our prediction of the conditions at break-up,  $G = 0.0541$ , with Grace's (1971) experimental observations in figure 7. In shear flow Grace saw drops breaking sometimes by tip streaming and sometimes by fracture. Our prediction is in fair agreement with the observed break up by fracture, except at the less small values of  $\lambda$ . At  $\lambda = 0.1$ , however, we predict an aspect ratio at break up of 4, which is not very large as assumed in our slender body theory. The difference in the power law between the experiments and our theory does not result from our assumption that the cross-section is circular because a slender body theory which calculates the correct cross-sectional shape would also produce a  $\lambda^{-2/3}$  prediction for break-up.

#### 4.5. A jump in shear rate

A number of experimental studies have reported that the measured critical shear rate beyond which no equilibrium could be found depends on the way the shear rate is changed, and that higher shear rates could be reached by increasing the shear rate more slowly (Torza, Cox & Mason, 1972). To study this nonlinear aspect of the equilibria we have conducted a numerical experiment in which we start with an equilibrium drop shape corresponding to one shear rate  $G_0$  and then suddenly change the shear rate to a new value  $G_1$ .

In all the cases in which the shear rate was decreased,  $G_1 < G_0$ , the drop attained

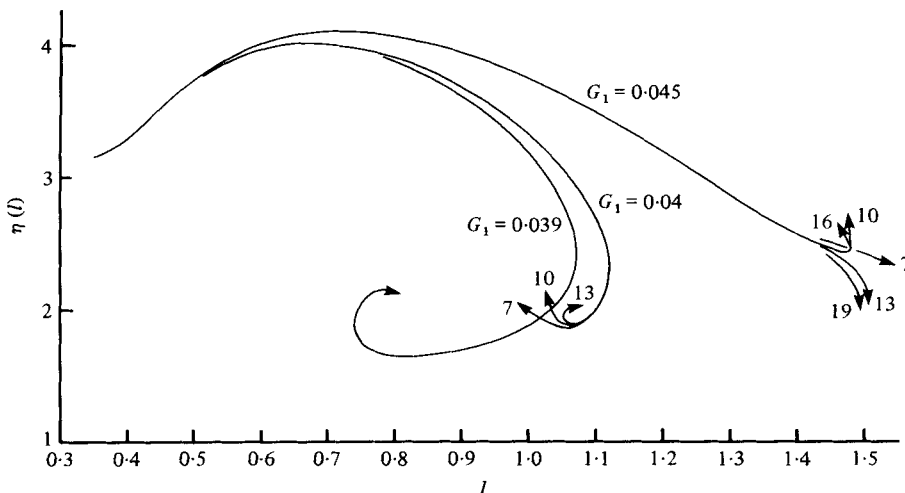


FIGURE 8. The path of the tip of the drop after a sudden jump in the shear rate from  $G_0 = 0.01$  to  $G_1 = 0.039, 0.04$  and  $0.045$ . The blobs along the curves are at time intervals of  $t = 0.1$ . The predictions of the different polynomial representations diverge after  $t = 1$  for  $G = 0.04$  and after  $t = 0.9$  for  $G = 0.045$ .

the equilibrium shape corresponding to the new shear rate  $G_1$ . When the shear rate was increased, the drop attained the equilibrium shape corresponding to the new shear rate so long as the jump was not too large. There was however, a critical value  $G_1^*$  such that the drop did not attain its equilibrium shape if the new shear rate exceeded this critical value, in spite of the existence of a stable (to small disturbances) equilibrium when the new shear rate lay in the range  $G_1^* < G_1 < 0.0541$ .

An example of the effect caused by a sudden increase in the shear rate is given by figure 8 which shows the path of the tip of the drop, the point  $x = l$  and  $y = \eta(l)$ , as a function of time after the shear rate has been increased from  $G_0 = 0.01$  to  $G_1 = 0.039, 0.04$  and  $0.045$ , the value of  $G_1^*$  being  $0.0396 \pm 0.0001$  for this  $G_0$ . In the case  $G_1 = 0.039$  which is less than  $G_1^*$ , the end of the drop quickly rises, then the drop extends until (for this just subcritical case) the length is roughly equal to that of the longest stable equilibrium, and finally the drop contracts to the stable equilibrium in a decaying oscillation. In the case  $G_1 = 0.04$  which is just above  $G_1^*$ , the drop roughly follows the  $G_1 = 0.039$  curve, but at time  $t = 1$ , just after the drop has started to contract to the stable equilibrium, the solution breaks down into a very rapid motion whose detailed form varies with the number of terms used in the polynomial representation. The case  $G_1 = 0.045$  shows no sign of contraction before  $t = 0.9$  when the solution breaks down. We do not understand this breakdown. It could be due to a spurious failure of the numerical representation, but this appears unlikely because all the representations agree well up to the breakdown, the nearby case  $G_1 = 0.039$  is represented with no difficulty, and also the polynomial representations easily reproduce the equilibria with  $l < 1.3$ . It is thus tempting to suggest that the breakdown is physically significant and might even be related to the observed phenomenon of tip-streaming (Grace 1971), because the details depend on the numerical representation of fine scales. The shape of the drop, however, shows no suggestive feature in the breakdown and certainly there is no hint of droplets streaming off the end. We regret

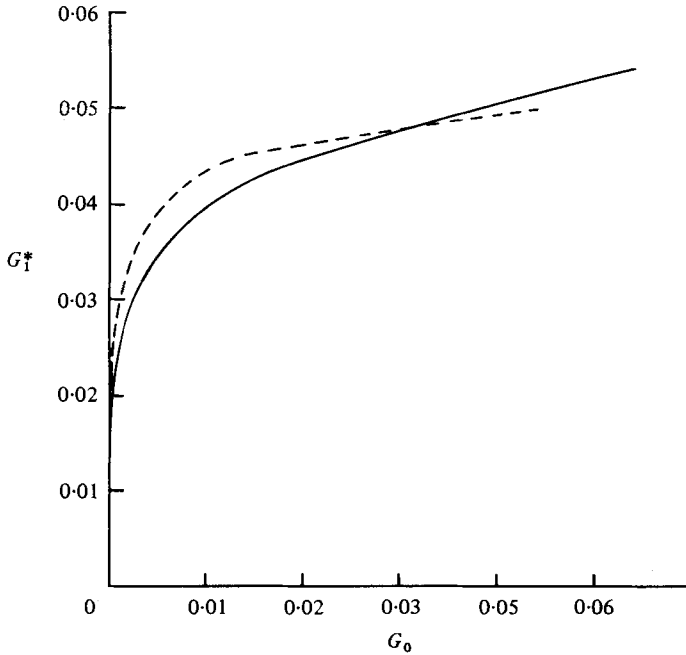


FIGURE 9. The marginal value of the new shear rate  $G_1^*$  as a function of the old shear rate to ensure that the drop attains the new equilibrium shape. The dashed curve is for the  $N = 1$  model.

that we can offer no physical understanding of this breakdown which occurs in our numerical experiments.

The dependence of the critical value of the new shear rate  $G_1^*$  on the starting shear rate  $G_0$  is given in figure 9. The results were obtained with a 7-term representation, with spot checks with a 10-term representation. The dashed curve gives the results for our simple model, the 1-term representation, which differ from the exact results by about 10%.

The asymptotic behaviour of  $G_1^*$  as  $G_0 \rightarrow 0$  can be found in our simple  $N = 1$  model. We start from the equilibrium  $l = l_0 \sim 3.50G_0^{\frac{1}{2}}$ ,  $h = h_0 \sim 1.46G_0^{-\frac{1}{2}}$  as  $G_0 \rightarrow 0$ . In a first phase of the unsteady process of duration  $G_0^{\frac{1}{2}}$  (the time scale found in § 4.4 for the oscillations about the  $G_0$  equilibrium), the surface tension restoring force is  $O(G_0/G_1)$  and therefore negligibly small, assuming that we find  $G_1^* \gg G_0$  as  $G_0 \rightarrow 0$ . Thus the governing equations in the first phase are

$$\dot{l} = h \quad \text{and} \quad \dot{h} = 7.5l^{-2},$$

with solution

$$h^2 = 3h_0^2 - 15l^{-1},$$

$$(l^2 - \frac{2}{3}l_0)^\frac{1}{2} - 3^{-\frac{1}{2}}l_0 + \frac{2}{3}l_0 \ln \frac{l^\frac{1}{2} + (l - \frac{2}{3}l_0)^\frac{1}{2}}{l_0^\frac{1}{2}(1 + 3^{-\frac{1}{2}})} = 3^\frac{1}{2}h_0 t.$$

Thus we leave the first phase with the end of the drop being advected with the flow at a height  $3^\frac{1}{2}$  higher than at the start. As the drop lengthens the surface tension restoring term in the  $\dot{l}$  equation grows to a maximum of  $0.125G_1^{-1}$  at  $l = 1.08$ , while the advection term is  $2.54G_0^{-\frac{1}{2}}$  until  $h$  decreases. As we are interested in the marginal

case  $G_1^*$  where the surface tension restoring term and the advection term are comparable, we are led to consider  $G_1 = O(G_0^{\frac{1}{2}})$ . Thus the second phase has a duration  $G_0^{\frac{1}{2}}$  in which  $l = O(1)$  and  $h = O(G_0^{-\frac{1}{2}})$ . If we set  $t = 4.472G_1T$  and  $h = 2.536G_0^{-\frac{1}{2}}H$ , the governing equations for the second phase are at lowest order

$$l_T = \beta H - l^{\frac{3}{2}}/(1 + 0.8l^3),$$

$$H_T = -Hl^{\frac{1}{2}}/(1 + 0.8l^3),$$

in which  $\beta = 11.340G_1/G_0^{\frac{1}{2}}$ . These equations must be solved numerically with initial conditions from the first phase  $H = 1$  and  $l = 0$  at  $T = 0$ . The numerical solutions show that the drop extends indefinitely if  $\beta > 2.073$ , while it contracts towards the equilibrium  $l = H = 0$  in this scaling if  $\beta < 2.073$ . Thus we predict from this matched asymptotic analysis that  $G_1 = 0.1828G_0^{\frac{1}{2}}$ , which is within 10% of the exact 1-term results for  $G_1 < 0.03$  and within 1% for  $G_1 < 0.015$ .

The numerical results of the more accurate representations show the same structure as our simple model as  $G_0 \rightarrow 0$ . As  $G_0 \rightarrow 0$ , the initial equilibrium shape has  $l = O(G_0^{\frac{1}{2}})$  as found in §3.2 and, by the volume constraint,  $\eta$  and  $R$  are both  $O(G_0^{-\frac{1}{2}})$ . When the shear rate is suddenly increased to  $G_1$ , the end of the drop rises by a small numerical factor in a time  $O(G_0^{\frac{1}{2}})$ , and the drop is then advected with the flow with  $\eta = O(G_0^{-\frac{1}{2}})$ . The end rises because of the tapering which diminishes as the drop lengthens. As the drop extends, the advection term  $\eta R'$  in the  $\dot{R}$  equation drops like  $G_0^{-\frac{1}{2}}l^{-\frac{3}{2}}$  from being initially  $O(G_0^{-1})$  to being  $O(G_0^{-\frac{1}{2}})$  at  $l = 1$ , while the internal pressure term grows like  $G_0^{-\frac{1}{2}}l^{\frac{3}{2}}$ , from being initially negligibly small to being  $O(G_0^{-\frac{1}{2}})$  at  $l = 1$ . Thus the surface tension term  $1/2G_1$  must stop the extension when  $l = O(1)$ , or sooner, by having  $G_1 < O(G_0^{\frac{1}{2}})$  if it is going to be effective. The numerical results do show that  $G_1^* \sim 0.15G_0^{\frac{1}{2}}$  as  $G_0 \rightarrow 0$  and that just below the marginal case the drop is stretched to roughly the length of the largest stable equilibrium  $l = 1.13$  before contracting to the equilibrium with  $l = O(G_1^{\frac{1}{2}})$ . Just above the marginal case however the more accurate representations show that the drop does not extend indefinitely as in the 1-term representation but instead the drop begins to contract before the solution breaks down at a well determined time.

This work was supported in part by the National Science Foundation under grants ENG-23229 and by a NATO research grant 1442. It was initiated at Cambridge while A. Acrivos was on sabbatical under a Guggenheim fellowship. The authors wish to thank Mr H. P. Grace of the Dupont Company for providing them with a summary - figure 7 - of his unpublished experimental work.

#### REFERENCES

- ACRIVOS, A. & LO, T. S. 1978 *J. Fluid Mech.* **86**, 641.  
 BUCKMASTER, J. 1972 *J. Fluid Mech.* **55**, 385.  
 BUCKMASTER, J. 1973 *Trans. A.S.M.E. E, J. Appl. Mech.* **40**, 18.  
 COX, R. G. 1969 *J. Fluid Mech.* **37**, 601.  
 GRACE, H. P. 1971 *Eng. Found. 3rd Res. Conf. on Mixing, Andover, N.H.*  
 HINCH, E. J. & ACRIVOS, A. 1979 *J. Fluid Mech.* **91**, 401.  
 TORZA, S., COX, R. G. & MASON, S. G. 1972 *J. Colloid Interface Sci.* **38**, 395.